

Robot self-calibration using multiple kinematic chains

Karla Stepanova^{1,2} and Matej Hoffmann²

Abstract—Proper calibration is key for the performance of every robot. Pushed by societal needs and economic opportunities, robots are leaving fixed factory floors and are deployed in more versatile ways both in industry and outside, which increases the need for automated calibration procedures. At the same time, advances in sensor technology make affordable but increasingly accurate devices such as RGB-D and tactile sensors available, making it possible to perform automated self-contained calibration relying on redundant information in these sensory streams. In this work, we take the example of a humanoid robot with a stereo camera system and force-sensitive end-effectors and quantitatively compare the performance of kinematic calibration by employing different combinations of intersecting kinematic chains—either through self-observation or self-touch.

I. INTRODUCTION

Practically all robots performing manipulation tasks rely on models of their bodies and their success is largely determined by their accuracy. However, inaccuracies creep in many ways as for example in the assembly process, in mechanical elasticity, or simply because of cheap design of components. Therefore, the actual model parameters of every robot exemplar have to be found by means of a calibration procedure, usually relying on external metrology system. For kinematic calibration, such apparatuses can measure one or more of the components of the end-effector pose employing mechanical, visual, or laser systems (see [1] for a survey). Different arrangements have different calibration index, accuracy, requirements on the environment, and cost. Standard robot calibration procedures require to know beforehand a number of quantities from the robot’s environment (such as a measurement system with a known pose w.r.t. the robot base, a fixed contact point in the environment where the robot can be attached, a surface that is known to be planar on which the robot can slide, etc.). These conditions have to be present for recalibration to be performed.

However, current trends in the robotics industry make the classical calibration procedures less practical: with the advent of the so-called “collaborative robots”, for example, the machines are becoming cheaper, lightweight, and compliant, and they are being deployed in more versatile ways according to the needs of customized production of smaller badges rather than being fixed in a single production line for their entire lifetime. All these factors increase the need for calibration to be performed more frequently and

¹Czech Institute of Informatics, Robotics, and Cybernetics, Czech Technical University, Prague, Czech Republic
karla.stepanova@cvut.cz

²Department of Cybernetics, Faculty of Electrical Engineering, Czech Technical University, Prague, Czech Republic.
matej.hoffmann@fel.cvut.cz

they are no less relevant for service robots operating in our homes. At the same time, the robots often come with richer sets of powerful sensory devices that are affordable and not difficult to operate. Both these trends speak for alternative solutions to the self-calibration problem that are more “self-contained” and can be performed autonomously by the robot, moving beyond the classical hand-eye calibration that arises when robot grippers are equipped with a camera. The main sensory devices available can be camera(s), RGB-D sensors (like Kinect), tactile sensors, and inertial sensors. As these typically not only provide information about the environment but also about the robot itself, they can be employed for self-calibration. The work of Dean-Leon et al. [2] deals with rapid deployment of a robot equipped with multimodal electronic skin.

In this work, we take the example of a humanoid robot with a stereo camera system and force-sensitive end-effectors and quantitatively compare the performance of kinematic calibration by employing different combinations of intersecting kinematic chains—either through self-observation or self-touch. The robot kinematics is represented using the standard Denavit-Hartenberg (DH) parameters. Hollerbach et al. [1] classify different calibration methods into *open-loop*—where one or more of the components of the end-effector pose is measured employing mechanical, visual, or laser systems—and *closed-loop* where physical constraints on the end-effector position or orientation can substitute for measurements.¹ Observing the end-effector—or in general any other points on the kinematic chain—using a camera falls into the open-loop calibration family, even though components of the end-effectors pose can be observed only indirectly through projection into the camera frame. The self-touch configurations—in this work end-effectors of the two arms in contact—can in our case be regarded as open-loop as well, since the contact does not act as a physical constraint but rather as measurement: a tactile or force sensor would signal that the two end-effectors are in the same position (i.e. one arm can be used to measure 3 components of the end-effector pose of the other arm).

Our work is motivated by calibration in the real world—like different approaches to kinematic calibration of the iCub humanoid robot relying on self-observation [4], self-touch [5], or inertial measurements [6]—but our contribution here is mostly theoretical. Our goal is to get insights into the pros and cons of different optimization problem formulations and answer questions like whether a “divide-and-conquer”

¹In fact, the open- and closed-loop formulation can be shown to be mathematically equivalent—the external measurement systems can be modeled as additional joints and links that close a virtual loop [3].

approach should be applied or whether it is beneficial to calibrate multiple chains simultaneously.

This article is structured as follows. Related work is reviewed in the next section, followed by Materials and Methods, Data Acquisition and Description, and Experimental Results. We close with a Discussion and Conclusion.

II. RELATED WORK

We mainly focus on humanoid robots or humanoid-like setups. With two arms and many Degrees of Freedom (DoF) that can possibly self-touch, a stereo camera, and other sensors like tactile or inertial, they are on one hand challenging to calibrate but at the same time, the possibilities for automated self-contained calibration are the greatest.

Most often, the loop is closed through self-observation of the end-effector using cameras located in the robot head (*open-loop calibration* method per [1]). Hersch et al. [7] and Martinez-Cantin et al. [8] present online methods to calibrate humanoid torso kinematics relying on gradient descent and recursive least squares estimation, respectively. The iCub humanoid was employed in [9], [4]. Vicente et al. [9] used a model of the hand's appearance to estimate its 6D pose and used that information to calibrate the joint offsets. Fanello et al. [4] had the robot observe its fingertip and learned essentially a single transformation only to account for the discrepancy between forward kinematics of the arm and the projection of the finger into the cameras. Other works dealing with hand-eye kinematic chains are [10], [11].

Next to cameras, inertial sensors also contain information that can be exploited for calibration. Kinematic calibration was shown exploiting 3-axis accelerometers embedded in the artificial skin modules distributed on robot body [12], [2] or in the control boards on the iCub [6].

Another family of approaches exploits some form of physical contact of the end-effector with the environment. One possibility is to attach the end-effector of a redundant manipulator to the ground, thereby fixing it in space. Even if the position is unknown, this constraint is sufficient for calibration by moving the manipulator and relying on encoder information only—see [13] who also show that this is equivalent to rigidly connecting two manipulators (that need to have together at least 7 DoF). The environmental constraints can take other forms as well like the triangular artifact with spheres mounted on it that the robot contacts using a touch probe [14]. The environmental constraints can also be learned online forming a contact manifold [15]. All these fall into the *closed-loop calibration* category [1] and require some form of force sensing on the part of the manipulator.

The advent of robotic skin technologies [16], [17], [18] opens up the possibility of a new family of approaches, whereby the chain is also closed through contact, but this time not confined to the end-effector. Furthermore, the contact position can be extracted from the tactile array. Roncone et al. [5] showed this on the iCub robot that performs autonomous self-touch using a finger on the contralateral arm; Li et al. [19] employed a dual KUKA arm setup with

a sensorized “finger” and a tactile array on the other manipulator. Forward kinematics together with skin calibration provide contact position that be then used for calibration. In this sense, the skin provides a pose measurement rather than constraint and as such, this may fall under *open-loop calibration*. In this way, one arm of a humanoid can be used to calibrate the other. Khusainov et al. [20] exploit this but using an industrial manipulator to calibrate the legs of a humanoid robot.

Birbach et al. [21] were to our knowledge the only ones to employ truly “multisensorial” or “multimodal” calibration. Using the humanoid robot Justin observing its wrist, the error functions comparing the wrist's position from forward kinematics with its projection into the left and right camera images, Kinect image, and Kinect disparity, together with an inertial term, were aggregated into a single cost function to be minimized. It is claimed that while pair-wise calibration can lead to inconsistencies, calibrating everything together in a “mutually supportive way” is most efficient.

In this work, we set out to both theoretically and empirically examine the pros and cons of different optimization problem formulations. In particular, we contrast: (i) calibration through self-observation (with projection into cameras) vs. calibration through self-touch; (ii) pair-wise optimization of kinematic chains with cross-calibration combining several chains at once. In both aspects, our work makes a unique contribution, also compared to [21] who, first, employ essentially only “hand-eye” kinematic chains terminating in different vision-like sensors in the robot head, and, second, do not compare their method with pair-wise calibration.

III. MATERIALS AND METHODS

A. iCub robot kinematic model

In this work, we use the upper body of the iCub humanoid robot (see Figure 1) and its kinematic model expressed in the Denavit-Hartenberg convention, where every link i is described by 4 parameters: $\{a_i, d_i, \alpha_i, o_i\}$. In this platform, all joints are revolute. We will consider several kinematic chains: all start in a single inertial or base frame—denoted iCub *Root* reference frame here. For every chain, the DH parameters and the DH convention itself uniquely define a chain of transformation matrices from the inertial frame to the end-effector. The position and orientation of the end-effector in the *Root* frame is thus given by $T_n^{Root} = A_1(q_1) \dots A_n(q_n)$ where the homogeneous transformation matrices A_i can be constructed from the DH representation and q_i are current joint angles of the robot actuators.

We will consider four basic kinematic chains which all originate in a common base frame and we will denote it the *Root* frame. The links are schematically illustrated in Figure 1. iCub kinematics version 1 was used [22] with the following modification: the *Root* was moved from the waist area to the third torso joint, which is the new inertial frame for our purposes.

The four chains under consideration are:

1) Left arm (LA). The DH parameters are in Table I.

We will use the following short names to denote the

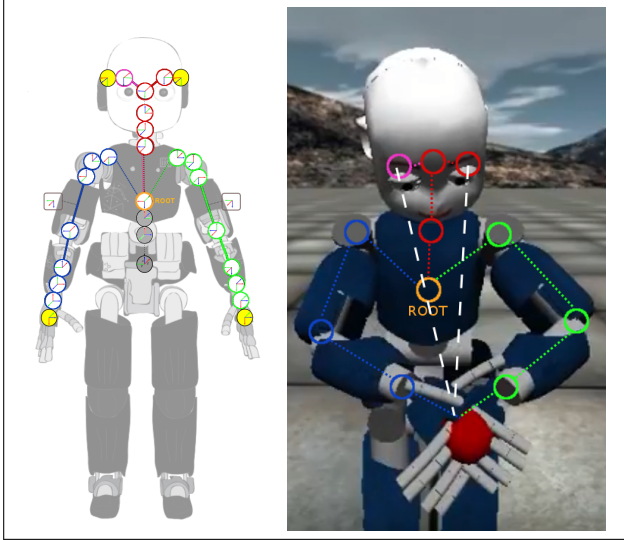


Fig. 1: iCub upper body and schematic illustration of kinematic chains considered. All chains originate in a common *Root* which is located at the third torso joint. The left and right arm chains are drawn in green and blue respectively. The eye chains have a common Root-to-head chain part marked in red. The right panel illustrates the self-calibration by connecting different chains—self-touch and self-observation. White lines denote projection into eyes.

links/joints: ROOT, LA shoulder pitch, LA shoulder roll, LA shoulder yaw, LA elbow, LA wrist prosup, LA wrist pitch, LA wrist yaw.

- 2) Right arm (RA). The DH parameters are analogous to LA (see [22]). The link/joint names: ROOT, RA shoulder pitch, RA shoulder roll, RA shoulder yaw, RA elbow, RA wrist prosup, RA wrist pitch, RA wrist yaw.
- 3) Left eye (LEye). DH parameters in Table II. Link/joint names: ROOT, neck pitch, neck roll, neck yaw, eyes tilt, left eye pan.
- 4) Right eye (REye). DH parameters different than LEye in Table III. Link/joint names:= ROOT, neck pitch, neck roll, neck yaw, eyes tilt, right eye pan.

Link(i)	a(i) [mm]	d(i) [mm]	α [$^\circ$]	o [$^\circ$]
1	23.36	143.3	$\pi/2$	$105 * \pi/180$
2	0	107.74	$-\pi/2$	$\pi/2$
3	0	0	$\pi/2$	$-\pi/2$
4	15	152.28	$-\pi/2$	$75 * \pi/180$
5	-15	0	$\pi/2$	0
6	0	137.3	$\pi/2$	$-\pi/2$
7	0	0	$\pi/2$	$\pi/2$
3	62.5	-16	0	0

TABLE I: DH parameters (a, d, α and offsets o describing all links in Left arm kinematic chain, starting with the Link 1 connecting the ROOT and the shoulder joint.

B. Optimization problem formulation

By calibration we mean estimation of the parameter vector $\phi = \{[a_1, \dots, a_n], [d_1, \dots, d_n], [\alpha_1, \dots, \alpha_n], [o_1, \dots, o_n]\}$ with

Link(i)	a(i) [mm]	d(i) [mm]	α [$^\circ$]	o [$^\circ$]
1	2.31	-193.3	$-\pi/2$	$\pi/4$
2	33	0	$\pi/2$	$\pi/4$
3	0	1	$-\pi/2$	$\pi/4$
4	-54	82.5	$-\pi/2$	$\pi/4$
5	0	-34	$-\pi/2$	0
6	0	0	$\pi/2$	$-\pi/4$

TABLE II: DH parameters (a, d, α and offsets o describing all links in the Left eye kinematic chain, starting with the Link 1 connecting the ROOT and the first neck joint.

Link(i)	a(i) [mm]	d(i) [mm]	α [$^\circ$]	o [$^\circ$]
5	0	34	$\pi/2$	$-\pi/4$
6	0	0	$-\pi/2$	0

TABLE III: DH parameters (a, d, α and offsets o describing all links in the right eye kinematic chain, Link 1-4 are shared with the Left eye kinematic chain.

$i \in N$, where $N = \{1, \dots, n\}$ is a set of indices identifying individual links, a, d and α are the first three parameters of the DH formulation [23], and o representing the offset that specifies the positioning of the encoders on the joints with respect to the DH representation. We often estimate a subset of these parameters only, assuming that the others are known. This subset can for example consist of a subset of joints $N' \subset N$ (i.e., only parameters of one arm of a humanoid robot are to be calibrated) or a subset of the parameters (i.e., only offsets o are to be calibrated – sometimes dubbed “daily calibration” [11]).

The estimation of the parameter vector ϕ is done by optimizing a given objective function:

$$\phi^* = \underset{\phi}{\operatorname{argmin}} \sum_{m=1}^M \|p_m^r - p_m^e(\phi, \Theta_m, \zeta)\|, \quad (1)$$

where M is number of end-effector poses used for calibration, p_m^r is a real end-effector pose, p_m^e is an estimated end-effector pose computed using a given parameter estimate ϕ , joint angles from joint encoders Θ_m and other parameters ζ (camera calibration parameters etc.).

C. Kinematic chain calibration

We study different combinations of intersecting chains and their performance in calibrating one another.

1) *Two arms chain (LA-RA)*: This corresponds to the self-touch scenario, with touch occurring directly at the end-effectors. The newly established kinematic chain for upper body includes both arms while head and eyes are excluded. To optimize parameters describing this chain, we minimize the distance between estimated positions in 3D space of left and right arm end-effectors. In this case, the parameter vector ϕ consists of the following parameters: $\phi = \{\phi^r, \phi^l\}$, where ϕ^r and ϕ^l are parameters corresponding to the robot right and left arm, respectively. The objective function to be optimized is then defined as follows:

$$\phi^* = \underset{\phi}{\operatorname{argmin}} \sum_{m=1}^M \|X_m^{r,R}(\phi^r, \Theta_m^r) - X_m^{l,R}(\phi^l, \Theta_m^l)\| \quad (2)$$

where M is a number of end-effector poses used for calibration, $X_m^{r,R}$ and $X_m^{l,R}$ are the m th estimated end-effector poses in the Root frame for the right and left arm, respectively, computed using a given parameter estimate ϕ and joint angles from joint encoders Θ_m .

2) *Hand to eye chains (LA-LEye, LA-REye, RA-LEye, RA-REye)*: There are in general two main options how to create a closed hand-to-eye kinematic chain. Both of them make use of visual measurement system of the robot.

The first option, used here, is to predict position of the end-effector in each of the robot cameras (similar to [21]). The estimated end-effector position is given by a current hypothetical robot calibration of the parameter vector ϕ and is computed via forward kinematics. The estimated end-effector position (X^{Root}) is mapped to left camera coordinates (X^{LEye}) using a transformation matrix T_{Root}^{LEye} . Then we use a pinhole camera model to transform the achieved 3D point (X^{LEye}) into image coordinates (X^{img}):

$$\begin{pmatrix} X_x^{img} \\ X_y^{img} \end{pmatrix} = \begin{pmatrix} f d_K X_x^{LEye} / X_z^{LEye} \\ f d_K X_y^{LEye} / X_z^{LEye} \end{pmatrix}, \quad (3)$$

where f is the focal length of the camera and d_K is radial distortion.

This approach doesn't require information from both eyes and enables us to estimate only one side of the robot body (e.g. parameters of the left arm and left eye). For example, the estimated parameter vector ϕ in the case of the kinematic chain connecting left arm and left eye consists of the following parameters: $\phi = \{\phi^l, \phi^{le}\}$, where ϕ^l and ϕ^{le} are parameters corresponding to the robot left arm and to the left eye, respectively. The objective function is then defined as:

$$\phi^* = \underset{\phi}{\operatorname{argmin}} \sum_{m=1}^M \|X_m^{img}(\phi^l, \phi^{le}) - u_m^L\|, \quad (4)$$

where X_m^{img} is th m th 2D position of the estimated left arm end-effector projected to left eye image coordinates and u_m^L is the m th 2D position of the observed left arm end-effector in the left eye camera. For two arms and two eyes we get four possible combined chains: left arm to right eye, left arm to left eye, right arm to left eye and right arm to right eye. Since the results are similar due to symmetry, we present in the experimental section results only for the Left arm - Left eye (LA-LEye) chain.

The second option is for rectified images to reproject observed position of the end-effector in image coordinates of both eyes (pixel (u, v)) to 3D space (X^{eye}) (similar to [4], [24]). This constitutes our future work.

3) *Combining multiple chains (LA-RA-LEye, LA-RA-LEye-REye)*: In order to estimate all kinematic parameters of the robot, we can take advantage of combining all the above mentioned kinematic chains (or some of them) together.

For example in the case that we combine LA-RA, LA-LEye and LA-REye chains together into LA-RA-LReye, the estimated parameter vector ϕ consists of the following parameters: $\phi = \{\phi^r, \phi^l, \phi^{re}, \phi^{le}\}$, where $\phi^l, \phi^r, \phi^{re}$ and ϕ^{le} are parameters corresponding to the left arm, right arm,

right eye, and left eye, respectively. The objective function is in this case defined as:

$$\phi^* = \underset{\phi}{\operatorname{argmin}} \sum_{m=1}^M \{ \|X_m^{r,R}(\phi^r, \Theta_m^r) - X_m^{l,R}(\phi^l, \Theta_m^l)\| + \|X_m^{l,I}(\phi^l, \phi^{le}) - u_m^L\| + \|X_m^{r,I}(\phi^r, \phi^{re}) - u_m^R\| \}, \quad (5)$$

where M is a number of end-effector poses used for calibration, $X_m^{r,R}$ and $X_m^{l,R}$ are the m th estimated end-effector poses in the Root frame for the right and left arm, respectively. These are computed using a given parameter estimate ϕ and joint angles from joint encoders Θ_m . Values $X_m^{l,I}$ and $X_m^{r,I}$ are the m th positions of the estimated left arm end-effector projected to left eye and right eye image coordinates, respectively, and u_m^L and u_m^R are the m th 2D position of the observed left arm end-effector in the left eye and right eye camera, respectively.

D. Non-linear least squares optimization

The objective functions (Eqs. [1]- [5]) defined for the optimization problem described in Section III-B are of the least-squares form and therefore can be minimized by Lavenberg-Marquardt algorithm for nonlinear least squares optimization (we used MATLAB implementation of the algorithm). This iterative local algorithm performs minimization of a nonlinear objective function by linearizing at the current estimate every iteration. It interpolates between the Gauss-Newton and gradient descent method and combines advantages of both methods.

E. Error metrics

For comparing results achieved for individual settings we make use of the following error metrics:

1) *Cartesian error between poses (position)*: Cartesian position error E_c between two generic poses, A and B, where P_A and P_B are 3D Cartesian positions of the end-effector, is given by the following equation:

$$E_c = \sqrt{(x_A - x_B)^2 + (y_A - y_B)^2 + (z_A - z_B)^2}. \quad (6)$$

We evaluate the Cartesian error over the set of N testing poses, which are selected as described in the section IV-B.

2) *Quality of estimated parameters*: For each estimated parameter a_i we compute the mean difference (e_i) of the estimated parameter a_i^e from the target parameter value a_i^t (averaged over R repetitions of the experiment):

$$e_i = \frac{\sum_{r=1}^R |a_{i,r}^e - a_i^t|}{R}, \quad (7)$$

as well as standard deviation of the parameter.

IV. DATA ACQUISITION AND DESCRIPTION

A. Pose set generation

With the goal of comparing different calibration methods in a humanoid robot, we chose a dataset where the two arms of the robot are in contact—thereby physically closing

the kinematic chain through self-touch—and at the same time the robot gazes at the contact point (self-observation). Different to [5] where a special inverse kinematics solver was developed for generating the self-touch configurations by forming a single floating-base chain composed of the two arms, here we employed the standard Cartesian arm and gaze solvers and controllers available for the iCub robot [25], [26]. A cubic volume in the robot’s workspace was chosen and then sampled with 20 points per dimension, giving rise to 8000 points in Cartesian space to which both arms and the head-eye plant were commanded (details and a video can be accessed at [27]). The full dataset thus consists of 8000 data vectors $X_i = [X_i^{target}, X_i^{RA}, X_i^{LA}, \Theta_i^j]$ composed of target point coordinates ($X_i^t \in \mathbb{R}^3$), corresponding right arm ($X_i^{RA} \in \mathbb{R}^3$) and left arm end-effector positions ($X_i^{LA} \in \mathbb{R}^3$), and joint angles Θ_i^j for every joint of the torso, arms, neck, and eyes, j ($\Theta_i^j \in \mathbb{R}$). Note that the solvers work with a given tolerance and hence $X_i^{target} \neq X_i^{RA} \neq X_i^{LA}$. Instead, there is a distribution of small errors as shown in Figure 2.

This way of dataset generation is a shortcut that is acceptable for the analysis that follows. In a real robot, one would require tactile or force sensing on the part or parts to be touched and a controller that would safely bring the robot parts into contact even if the kinematic model contains errors. Li et al. [19] employ tactile servoing in a dual KUKA arm setup. The actual contact points will have to be measured using the tactile devices and the kinematic chains under calibration extended with these additional transformations from the last link of the DH chain [19], [5]. In this case, the accuracy of the calibration will depend on the accuracy of the skin calibration.

B. Training and testing dataset

For our experiments, we selected 1000 best configurations with $|X_i^{RA} - X_i^{LA}| < 0.0001$ mm – called D in what follows. The 0.0001mm error will at the same time constitute the lower bound on the maximum achievable calibration accuracy using the closure of the kinematic chain through self-touch. For the case of loop closure through the cameras, this is not the case since we will project the end-effector positions directly and accurately into the cameras simulated in Matlab. The 1000 data points selected were further divided into training and testing datasets in the following way: N out of the best 700 poses are used as a training set on which the optimization process is performed and 300 poses are used for testing purposes.

In Figure 3 we show the distribution of joint values for individual joints (1000 selected configurations).

C. Perturbation of the initial parameters estimate

To evaluate the dependence of the optimization performance on the quality of the initial estimates of the parameters, we perturbed all estimated parameters by some given value (*degree of perturbation* p). We perturbed all initial offset values o_i as follows:

$$o_i^{new} = p * uniform[-1; 1] + o_i, \quad (8)$$

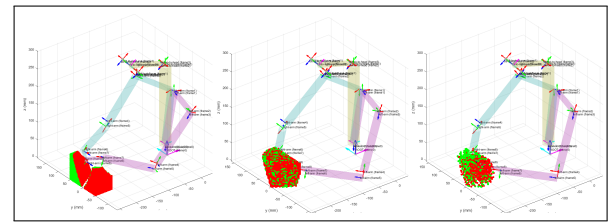


Fig. 2: Dataset visualization. Red points – left arm end-effector positions; Green points – right arm. Data points divided according to distance $d = |X_i^{RA} - X_i^{LA}|$ in mm. (left) 2500 data points with $d > 0.1$; (middle) 5500 data points with $0.0001 < d \leq 0.01$; (right) 1000 selected data points with $d \leq 0.0001$.

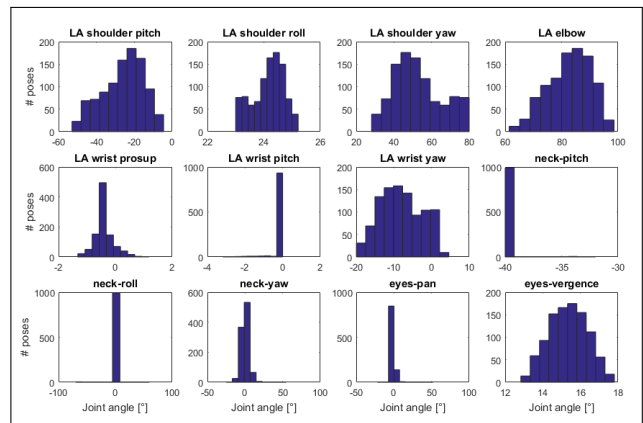


Fig. 3: Dataset - distribution of joint values over the acquired dataset (we show values for the 1000 selected configurations)

It is reasonable to expect that the remaining DH parameters (a , d and α) will be in general more accurate as they can be extracted from CAD models and there is no moving part and no encoder involved. Therefore, their perturbation was reduced by a factor of 10:

$$\Phi_i^{new} = 0.1 * p * uniform[-1; 1] + \Phi_i, \quad (9)$$

for $p = \{2, 5, 10, 20\}$.

V. EXPERIMENTAL RESULTS

In this section, we show our calibration results. We evaluated our approach using both an error of the end-effector position—the cost function optimized (or distance in camera frame for projections into eyes)—as well as error in individual parameters (against their correct values). We compared different degree of perturbation on individual parameters, number of training poses (data points), as well as number of free parameters which were estimated by the optimization process. A summary Table IV presents the error on the testing dataset for individual settings. Free parameters (being calibrated) in a given chain are denoted with a check mark. That is, in the first row, we used the LA-RA connected chains (self-touch) for calibration we calibrated only parameters of the left arm (the right arm was considered to be known). All values in the table are shown in millimeters and averaged

over 10 repetitions. From the table, we can easily see which chains have the biggest troubles with the smaller number of training poses or higher value of perturbation on the estimated parameters. We present only results for lower number of training poses, because for 700 poses all compared methods (apart of LA-LREye chain) were able find a correct estimate of kinematic parameters (error was below the bound for achievable calibration accuracy). In the case of 700 poses, results didn't depend on the perturbation of the parameters and for all degrees of perturbation we, were able to find the optimum estimate of the parameters.

To visualise distribution of errors for individual chains, we plotted residua for each testing pose (error for each testing pose in x and y coordinates). The comparison over individual chains and number of poses is shown in Figure 4. For higher number of poses and lower perturbation of parameters, residuals have a zero mean and Gaussian distribution. For lower number of poses and especially for higher perturbation, the residuals are bigger and skewed. This is true especially for the LA-LEye chain which doesn't converge to the optimal solution for bigger initial parameter perturbation. For the lower number of poses, the resulting calibration also strongly depends on initialization. Therefore, we show residuals for 10 repetitions with random initialization for each condition.

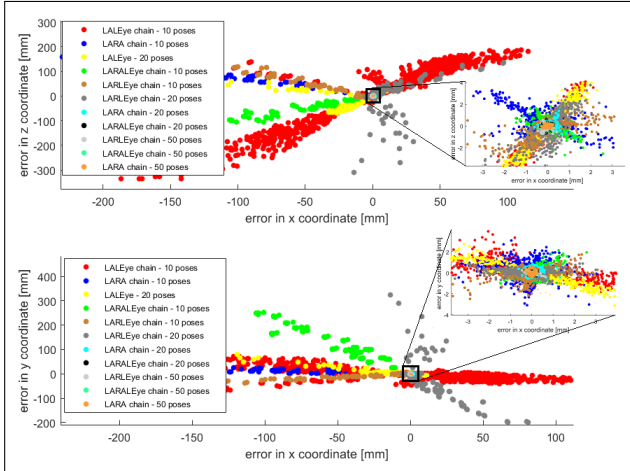


Fig. 4: Showing error residuals at end-effector on 3000 testing poses (visualized results on 300 poses for each of 10 repetitions) for individual chains and different number of training poses. (Top) Residuals in x and z coordinates. (Bottom) Residuals in x and y coordinates.

Chains that include eyes have shown the poorest performance, especially for higher perturbation of parameters and lower number of poses. This can be easily explained, because in the case of arm-one-eye-chain (like LA-LEye), the 3D information about the end-effector position is not fully available. Residuals for testing poses for 10 repetitions for the case of LA-LEye chain parameters estimation are shown in the Figure 5. As can be seen in the Table IV, when we include both eyes to the optimization, with the discretion that eyes are properly calibrated, estimation of the hand position improves dramatically.

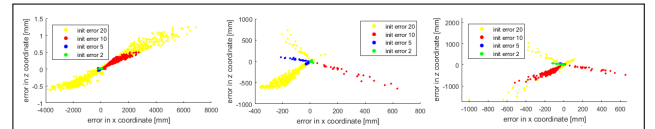


Fig. 5: Showing residuals on 3000 testing poses (visualised results on 300 poses for each of 10 repetitions) for individual connected chains and different number of training poses. (Left) 10 training poses; (Middle) 20 training poses; (Right) 50 training poses.

A. Quality of parameters estimates for LA-RA chain

We also evaluated the quality of individual parameter estimates. The true parameter values are optimized only indirectly as the optimized end-effector position is dependent on them. In Figure 6, we show results for all estimated parameters in case of the LA-RA chain when all the parameters are optimized. We can see that parameters a and d describing shoulder links are more accurate than the ones describing the wrist. This is expected as errors on distal joints affect the end-effector position more strongly.

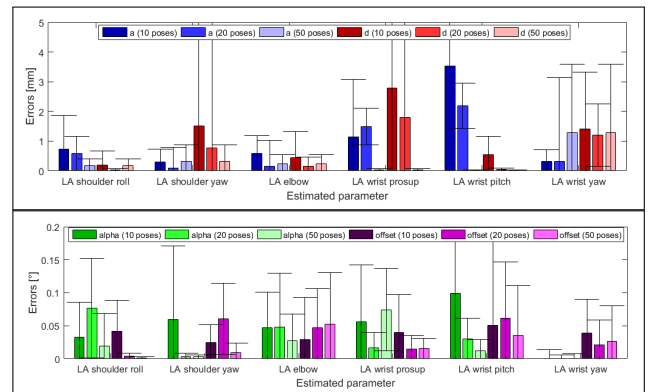


Fig. 6: Parameter estimation for left-arm-right-arm (LA-RA) chain. All parameters were estimated; only results for left arm shown due to symmetry. Errors of parameters after optimization for different number of poses: (Top) a and d DH parameters; (Bottom) α DH parameter and $offset$ (averaged over 10 repetitions, for initial degree of perturbation 10).

B. Multichain vs. pair-wise sequential calibration

Our next aim was to evaluate whether it is better to use one objective function which combines all estimated parameters and enables us to perform optimization in one step (as proposed in [21]) or to perform optimization sequentially using smaller kinematic chains (such as LA-RA, LA-LEye or RA-REye). Our results on this topic, albeit preliminary, do not confirm the hypothesis put forth by Birbach et al. [21] that multi-chain problem formulation would be beneficial. One of the results for perturbation degree 10 and 50 training poses can be seen in the Figure 8. Sequential calibration—LA-RA calibration for hands, then using these estimates as a first guess for the left arm parameters in LA-LEye and

TABLE IV: Evaluation of testing error over different settings (averaged over 10 repetitions)

Testing error [mm]	LA	RA	Parameters estimated		Perturbation degree			
			head	LEye	REye	2	5	10
10 poses	LA-RA	✓				2 ± 10	5 ± 33	3 ± 19
	LA-LEye	✓				13 ± 32	52 ± 67	323 ± 88
	LA-LREye	✓				1.0 ± 4.1	1.9 ± 6.2	6.5 ± 15.2
	LARALEye	✓				2 ± 11	7 ± 39	7 ± 34
	LA-RA	✓	✓			6 ± 11	10 ± 14	25 ± 53
	LARALEye	✓	✓			3 ± 10	7 ± 30	12 ± 30
	LA-LEye	✓	✓	✓		46 ± 550	67 ± 990	92 ± 1200
	LARALEye	✓	✓	✓		3 ± 8	1 ± 4	15 ± 40
	LA-LREye	✓	✓	✓	✓	63 ± 140	1354 ± 800	2688 ± 2000
	LARALEye	✓	✓	✓	✓	5 ± 15	9 ± 20	72 ± 154
20 poses	LARALREye	✓	✓	✓	✓	120 ± 118	210 ± 206	3119 ± 420
	LA-RA	✓				0	0	0
	LA-LEye	✓				2.6 ± 5.8	8.6 ± 17.0	7 ± 10
	LA-LREye	✓				1 ± 8	4 ± 17	17 ± 24
	LARALEye	✓				0	0	0
	LA-RA	✓	✓			1.5 ± 7.0	3 ± 10	5 ± 23
	LARALEye	✓	✓			2 ± 12	6 ± 31	5 ± 22
	LA-LEye	✓	✓	✓		25 ± 470	145 ± 400	602 ± 1600
	LARALEye	✓	✓	✓		1 ± 11	2 ± 34	10 ± 18
	LARALREye	✓	✓	✓	✓	33 ± 6	46 ± 18	59 ± 16
50 poses	LA-RA	✓				0	0	0
	LA-LEye	✓				1 ± 7	0.7 ± 4	37 ± 90
	LARALEye	✓				0	0	0
	LA-RA	✓	✓			0 ± 0	0.3 ± 0.3	0.4 ± 1.4
	LARALEye	✓	✓			0	0	0.3 ± 0.2
	LA-LEye	✓	✓	✓		15 ± 30	150 ± 170	142 ± 760
	LARALEye	✓	✓	✓		0.2 ± 0.1	0.7 ± 0.1	0.2 ± 0.1
	LARALEye	✓	✓	✓	✓	1 ± 30	3 ± 35	8 ± 26
	LARALREye	✓	✓	✓	✓	16.5 ± 0.2	15.9 ± 0.2	16.3 ± 0.2
	LARALREye	✓	✓	✓	✓			14.1 ± 5.2

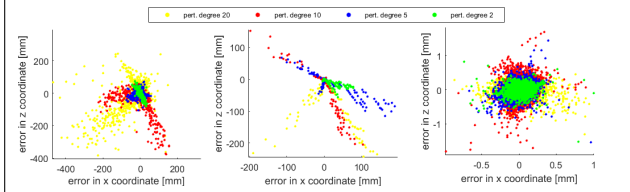


Fig. 7: Residuals for Left arm-right arm chain after calibration, visualising residuals on 300 testing poses for each of 10 repetitions (3000 testing poses in total), individual initial perturbation levels 2-20 for 10 training poses (left), 20 training poses (middle) and 50 training poses (right)

RA-REye chain, eye chain calibration then—achieved better estimates for parameters a and d and comparable results for the other parameters (α and o).

VI. DISCUSSION AND CONCLUSION

We investigated the pros and cons of different optimization problem formulations of the kinematic calibration problem. Overall, we could show that even for limited number of data points (training poses) and despite even large degree of initial parameter perturbations, good results can be obtained. For larger training data sets, the algorithm was able to find global optima. We specifically contrasted calibration through self-observation (with projection into cameras) vs. calibration through self-touch. Our results show that self-touch is indeed an effective self-calibration tool as 3 dimensions of the pose

can be observed. Finally, we have put the hypothesis proposed in [21] that calibrating multiple chains simultaneously is superior than pairwise sequential calibration to test. Our initial results do not confirm this, but further analysis is needed.

We have only reported results from simulation in Matlab, however, we claim that this was the right tool for this kind of study where our contribution is conceptual. At the same time, our analysis is firmly grounded in a real setting, since, first, we have employed the model of a real robot (iCub), and, second, the individual scenarios we analyzed were already demonstrated in the real robot—self-touch [5] and self-observation [4], [9] in particular.

There are several aspects that we want to further investigate in the future. First, the set of robot configurations was confined to a cubic volume in front of the robot where both arms can reach and self-touch is possible and, at the same time, the robot can gaze at this region. Such a dataset maximized the cross-calibration opportunities, however, it is likely that it did not excite some parameters optimally—at least for some of the chains involved. Observability and identifiability analysis will be desired as well as the possibility of active/optimal pose selection. Second, the information from the two cameras can be used also differently—rather than two projections into the camera frames one could employ the stereo system to “project rays” outwards—which will lead onto yet another formulation of the optimization problem. Finally, the self-touch scenario can be also turned

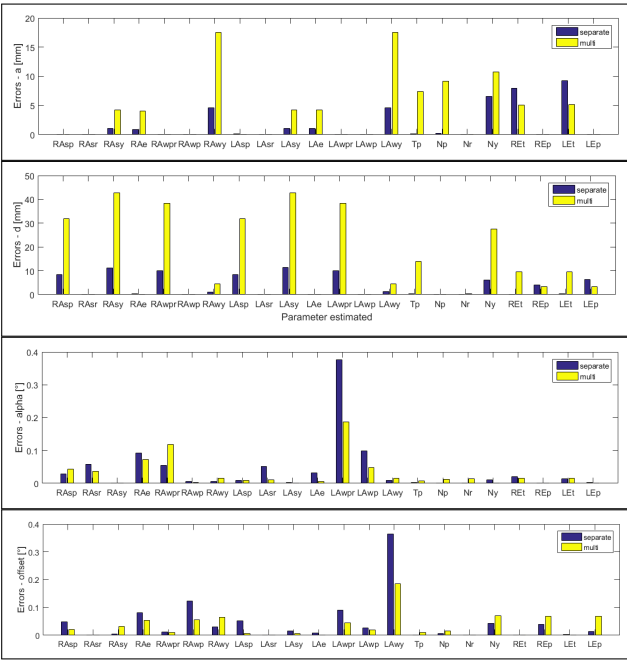


Fig. 8: Comparison of errors on individual DH parameters—multichain combining all chains in one objective function (multi – LA-RA-LEye-REye) vs. sequential calibration of smaller chains (LA-RA, LA-LEye, and RA-REye). From top to bottom: results for parameter a , d , α , and offsets are shown. X axis: shortcuts identifying individual joints in the iCub upper body. Initial degree of perturbation of all parameters was 10 and we used 50 training poses for optimization of parameters (results are averaged over 5 repetitions))

around from using some version of tactile array to calibrate kinematics [5], [19] to calibrating the skin itself [28].

ACKNOWLEDGMENT

This work was supported by the Czech Science Foundation under Project GA17-15697Y. We thank Alessandro Roncone for assistance with the models of the iCub robot in MATLAB and the source files leading to Fig. 1 left.

REFERENCES

- [1] J. Hollerbach, W. Khalil, and M. Gautier, “Model identification,” in *Springer Handbook of Robotics*, 2nd ed., B. Siciliano and O. Khatib, Eds. Springer, 2016, pp. 113–138.
- [2] E. Dean, K. R. Amaro, F. Bergner, I. Dianov, and G. Cheng, “Integration of robotic technologies for rapidly deployable robots,” *IEEE Transactions on Industrial Informatics*, 2017, [to appear].
- [3] J. Hollerbach and C. Wampler, “The calibration index and taxonomy for robotic kinematic calibration methods,” *International Journal of Robotics Research*, vol. 15(6), pp. 573–591, 1996.
- [4] S. R. Fanello, U. Pattacini, I. Gori, V. Tikhanoff, M. Randazzo, A. Roncone, F. Odone, and G. Metta, “3d stereo estimation and fully automated learning of eye-hand coordination in humanoid robots,” in *2014 IEEE-RAS Int. Conf. on Humanoid Robots - HUMANOIDS '14*, 2014.
- [5] A. Roncone, M. Hoffmann, U. Pattacini, and G. Metta, “Automatic kinematic chain calibration using artificial skin: self-touch in the iCub humanoid robot,” in *Robotics and Automation (ICRA), 2014 IEEE International Conference on*, 2014, pp. 2305–2312.
- [6] N. Guedelha, N. Kuppuswamy, S. Traversaro, and F. Nori, “Self-calibration of joint offsets for humanoid robots using accelerometer measurements,” in *Humanoid Robots (Humanoids), 2016 IEEE-RAS 16th International Conference on*. IEEE, 2016, pp. 1233–1238.
- [7] M. Hersch, E. Sauser, and A. Billard, “Online learning of the body schema,” *International Journal of Humanoid Robotics*, vol. 5, pp. 161–181, 2008.
- [8] R. Martinez-Cantin, M. Lopes, and L. Montesano, “Body schema acquisition through active learning,” in *Proc. Int. Conf. on Robotics and Automation (ICRA)*, 2010.
- [9] P. Vicente, L. Jamone, and A. Bernardino, “Online body schema adaptation based on internal mental simulation and multisensory feedback,” *Frontiers in Robotics and AI*, vol. 3, p. 7, 2016.
- [10] U. Hubert, J. Stuckler, and S. Behnke, “Bayesian calibration of the hand-eye kinematics of an anthropomorphic robot,” in *Humanoid Robots (Humanoids), 2012 12th IEEE-RAS International Conference on*. IEEE, 2012, pp. 618–624.
- [11] K. Nickels, “Hand-Eye calibration for Robonaut,” NASA Summer Faculty Fellowship Program Final Report, Tech. Rep., 2003.
- [12] P. Mittendorfer and G. Cheng, “Open-loop self-calibration of articulated robots with artificial skins,” in *Robotics and Automation (ICRA), 2012 IEEE International Conference on*. IEEE, 2012, pp. 4539–4545.
- [13] D. J. Bennett and J. M. Hollerbach, “Self-calibration of single-loop, closed kinematic chains formed by dual or redundant manipulators,” in *Decision and Control, 1988., Proceedings of the 27th IEEE Conference on*. IEEE, 1988, pp. 627–629.
- [14] A. Joubair and I. A. Bonev, “Kinematic calibration of a six-axis serial robot using distance and sphere constraints,” *The International Journal of Advanced Manufacturing Technology*, vol. 77, no. 1-4, pp. 515–523, 2015.
- [15] M. C. Koval, M. Klingensmith, S. S. Srinivasa, N. S. Pollard, and M. Kaess, “The manifold particle filter for state estimation on high-dimensional implicit manifolds,” in *Robotics and Automation (ICRA), 2017 IEEE International Conference on*. IEEE, 2017, pp. 4673–4680.
- [16] C. Bartolozzi, L. Natale, F. Nori, and G. Metta, “Robots with a sense of touch,” *Nature materials*, vol. 15, no. 9, pp. 921–925, 2016.
- [17] R. S. Dahiya and M. Valle, *Robotic Tactile Sensing*. Springer, 2013.
- [18] F. Mastrogiovanni, L. Natale, G. Cannata, and G. Metta, “Special issue on advances in tactile sensing and tactile-based human–robot interaction,” *Robotics and Autonomous Systems*, vol. 63, pp. 227–229, 2015.
- [19] Q. Li, R. Haschke, and H. Ritter, “Towards body schema learning using training data acquired by continuous self-touch,” in *Humanoid Robots (Humanoids), 2015 IEEE-RAS 15th International Conference on*. IEEE, 2015, pp. 1109–1114.
- [20] R. Khusainov, A. Klimchik, and E. Magid, “Humanoid robot kinematic calibration using industrial manipulator,” in *Mechanical, System and Control Engineering (ICMSC), 2017 International Conference on*. IEEE, 2017, pp. 184–189.
- [21] O. Birbach, U. Frese, and B. Bäuml, “Rapid calibration of a multi-sensorial humanoid upper body: An automatic and self-contained approach,” *The International Journal of Robotics Research*, vol. 34, no. 4-5, pp. 420–436, 2015.
- [22] 2017. [Online]. Available: <http://wiki.icub.org/wiki/ICubForwardKinematics>
- [23] J. Denavit, “A kinematic notation for lower-pair mechanisms based on matrices,” *Trans. of the ASME. Journal of Applied Mechanics*, vol. 22, pp. 215–221, 1955.
- [24] H. Hirschmuller, “Stereo processing by semiglobal matching and mutual information,” *IEEE Transactions on pattern analysis and machine intelligence*, vol. 30, no. 2, pp. 328–341, 2008.
- [25] U. Pattacini, F. Nori, L. Natale, G. Metta, and G. Sandini, “An experimental evaluation of a novel minimum-jerk cartesian controller for humanoid robots,” in *Proc. IEEE/RSJ Int. Conf. Int. Robots and Systems (IROS)*, 2010.
- [26] A. Roncone, U. Pattacini, G. Metta, and L. Natale, “A cartesian 6-dof gaze controller for humanoid robots,” in *Robotics: Science and Systems*, vol. 2016, 2016.
- [27] 2017. [Online]. Available: <https://github.com/matejhof/icub-selftouch-with-gaze-generator>
- [28] A. Albini, S. Denei, and G. Cannata, “Towards autonomous robotic skin spatial calibration: A framework based on vision and self-touch,” in *Intelligent Robots and Systems (IROS), 2017 IEEE/RSJ International Conference on*. IEEE, 2017, pp. 153–159.